

---

# OneLatent: Single-Token Compression for Visual Latent Reasoning

---

Bo Lv<sup>1\*¶</sup>, Yasheng Sun<sup>2\*</sup>, Junjie Wang<sup>1†</sup>, Haoxiang Shi<sup>3†</sup>

<sup>1</sup>Tsinghua University

<sup>2</sup>Institute of Science Tokyo

<sup>3</sup>Waseda University

boironic@gmail.com, sunyasheng01@yeah.net,  
wangjunjie@sz.tsinghua.edu.cn, hollis.shi@toki.waseda.jp

## Abstract

Chain-of-thought (CoT) prompting improves reasoning but often increases inference cost by one to two orders of magnitude. To address these challenges, we present **OneLatent**, a framework that compresses intermediate reasoning into a single latent token via supervision from rendered CoT images and DeepSeek-OCR hidden states. By rendering textual steps into images, we obtain a deterministic supervision signal that can be inspected and audited without requiring the model to output verbose textual rationales. Across benchmarks, OneLatent reduces average output length by 11 $\times$  with only a 2.21% average accuracy drop relative to textual CoT, while improving output token contribution (OTC) by 6.8 $\times$ . On long-chain logical reasoning, OneLatent reaches 99.80% on ProntoQA and 97.80% on ProsQA with one latent token, with compression up to 87.4 $\times$ , supporting compression-constrained generalization.

## 1 Introduction

Explicit chain-of-thought (CoT) prompting is one of the most effective ways to improve reasoning in language models [Wei et al., 2022, Wang et al., 2022b, Zhou et al., 2022, Khot et al., 2022, Wang et al., 2022a, Sprague et al., 2024], but it is expensive at deployment: output length, latency, and KV-cache usage all grow with generated reasoning tokens. More importantly, long traces are not always high-information traces; they often mix useful computation with template-like verbal redundancy [Turpin et al., 2024].

This motivates a minimum description length (MDL) view [Grünwald and Roos, 2019]: if two intermediate explanations both produce the correct answer, the shorter sufficient one can provide a stronger inductive bias and reduce redundant verbal scaffolding. However, MDL is not directly optimized in current CoT pipelines, which are trained with token-level likelihood on explicit traces rather than description length of internal reasoning states.

The challenge is that naive compression fails: weak compression keeps redundant verbal scaffolds, while aggressive compression removes task-critical computation. We therefore introduce a visual latent token: a learnable continuous latent slot whose representation is aligned to DeepSeek-OCR vision-encoder hidden-state targets derived from rendered CoT images [Wei et al., 2025a]. This differs from prior latent-reasoning approaches that stay in text space and typically allocate multiple latent tokens to carry intermediate computation. Importantly, the visual latent token is not an image

---

\* Equal contribution

† Corresponding author

¶ This work was performed when Bo Lv was visiting Tsinghua University as a research intern.

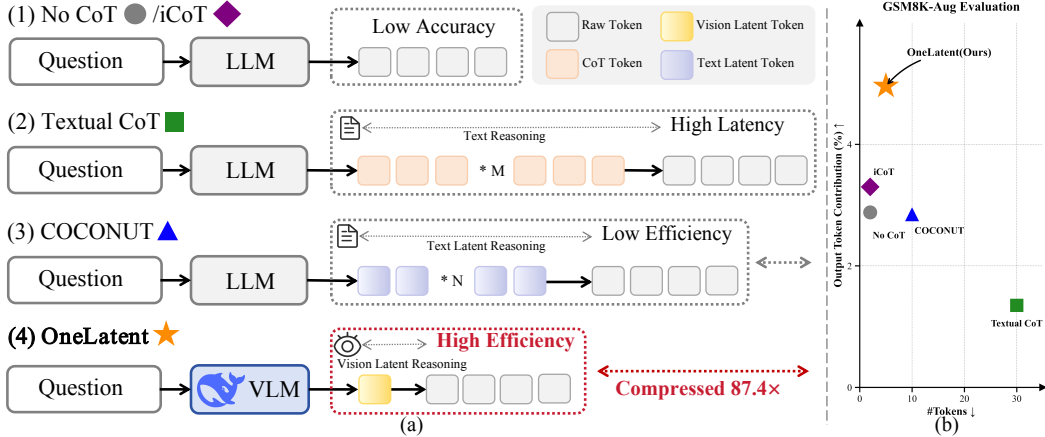


Figure 1: Reasoning interfaces and efficiency plot. (a) We illustrate four reasoning interfaces and their output forms: No CoT, textual CoT, iCoT, COCONUT, and OneLatent. (b) On GSM8K, we plot OTC (%/token) versus the average number of generated output tokens for the same methods. OneLatent appears in the lowest-output-length region and keeps high OTC, indicating substantially shorter outputs than the compared reasoning interfaces.

patch token at inference; test-time inputs contain only the question and a single latent slot before answer generation.

This aligns with the MDL intuition: under a strict intermediate-interface budget, the model is encouraged to represent only what is sufficient for answering. We do not optimize MDL explicitly; instead, we impose a single-latent interface and evaluate the resulting accuracy-length trade-off. Figure 1 (b) shows the resulting trade-off versus No-CoT, textual CoT, iCoT, COCONUT and OneLatent.

To quantify efficiency under constrained decoding, we introduce output token contribution (OTC), defined as  $OTC = \text{Acc}/\text{AvgOut}$ , where Acc is accuracy in percent and AvgOut is average generated output tokens (%/token). Unless noted otherwise, accuracy is macro-averaged across five benchmarks (GSM8K, GSM8K-Hard, SVAMP, ProntoQA, and ProsQA), and output length counts generated tokens excluding the prompt under identical decoding settings. Under this protocol, OneLatent reduces average output length from 74.62 to 6.78 tokens and incurs only a 2.21% macro-averaged accuracy drop relative to textual CoT, while improving OTC by 6.8x; in long-CoT settings, compression reaches up to 87.4x, with degradation concentrated in arithmetic-heavy tasks.

The main contributions are threefold:

- We propose a **visual-latent compression method** that uses DeepSeek-OCR hidden states to supervise one latent token with a stable three-stage curriculum.
- We propose an **MDL-motivated data preparation and CoT rendering strategy** that deterministically renders variable-length CoT into fixed-size images and compresses them into stable visual hidden-state targets for single-token latent supervision.
- We provide **evidence for compression-constrained generalization**: 11x output reduction with small accuracy loss, strong long-chain performance, and large gains in OTC as an MDL-motivated efficiency proxy.

## 2 Related Work

**Latent reasoning methods.** Recent work internalizes reasoning into hidden states to reduce token-level deliberation. iCoT [Deng et al., 2023, 2024], COCONUT [Hao et al., 2025], and related pause/latent-compute methods [Goyal et al., 2023, Zelikman et al., 2024, Pfau et al., 2024, Wei et al., 2025b] demonstrate that latent computation is feasible. However, these methods often show an accuracy gap relative to explicit CoT and can be sensitive to multi-stage optimization [Hao et al.,

2025]. Our approach keeps the latent interface minimal (single token) and uses external visual supervision to provide an inspectable, high-density target for guiding single-token distillation.

**Text-based reasoning methods.** Textual CoT and its variants remain strong baselines for multi-step reasoning [Wei et al., 2022, Wang et al., 2022b, Zhou et al., 2022, Khot et al., 2022, Wang et al., 2022a, Madaan and Yazdanbakhsh, 2022, Sprague et al., 2024]. Follow-up work improves reliability via verification, self-refinement, and search/planning at inference time [Shinn et al., 2023, Madaan et al., 2023, Wang et al., 2024, Xie et al., 2023, Hao et al., 2023, Yao et al., 2023, Hao et al., 2024, Wang et al., 2023, Valmeeekam et al., 2023, Welleck et al., 2024]. A key limitation is decoding cost: stronger performance often requires longer textual traces, and these traces are not always reliable indicators of the model’s internal computation and may include post-hoc or redundant content [Turpin et al., 2024]. OneLatent uses textual CoT as *training supervision* but removes it from the runtime interface.

**Visual context compression.** Visual compression methods encode long text segments as compact image representations. Glyph [Cheng et al., 2025] and DeepSeek-OCR [Wei et al., 2025a], together with strong vision-language encoders [Radford et al., 2021], show that visual channels can preserve dense textual semantics under aggressive compression. Prior work mainly targets context scaling or OCR quality, not latent reasoning supervision. We instead use optical compression as a bridge from long CoT traces to a single reasoning token, enabling compact inference while retaining much of the reasoning performance.

## 3 OneLatent Method

### 3.1 Overview

We transform explicit chain-of-thought reasoning into a single compressed latent token through a three-stage training curriculum: (1) explicit CoT Cold Start, (2) visual latent supervision via rendered CoT images, and (3) answer-only fine-tuning. We call this slot the visual latent token: the model learns to align this continuous slot with hidden-state targets extracted by a frozen vision-encoder from rendered CoT images.

Figure 2 illustrates the complete OneLatent pipeline, which consists of two main phases: an offline data preparation phase and an online three-stage training phase. Our target extraction follows the DeepSeek-OCR architecture, which includes a vision-encoder and an LLM backbone. In the data preparation phase, we render explicit CoT text into images using a deterministic layout algorithm, then extract hidden-state targets by passing these images through this frozen DeepSeek-OCR stack. These precomputed targets serve as supervision signals during training. In the three-stage training phase, we progressively compress reasoning: Stage 1 teaches the model to generate explicit CoT reasoning, Stage 2 aligns a single latent token to the visual hidden-state targets while removing explicit CoT generation, and Stage 3 fine-tunes answer generation to consolidate latent reasoning without alignment loss. At inference time, the model uses only the latent token to compress reasoning internally, generating short answers without explicit intermediate steps.

### 3.2 Latent Segment and Continuous Filling

Given a question  $q$  and answer  $a$ , we insert a latent segment between them:

$$x = [\text{BOS}, q, \underbrace{<|\text{begin-latent}|>, <|\text{latent}|>, \dots, <|\text{latent}|>, <|\text{end-latent}|>}_N, a, \text{EOS}]. \quad (1)$$

For all reported evaluations, we use  $N = 1$ . At latent positions, we overwrite the embedding with the previous hidden state. For latent position  $\ell$ :

$$e_\ell \leftarrow h_{\ell-1}, \quad h_\ell = f_\theta(e_{\leq \ell}). \quad (2)$$

This creates a continuous hidden-state “thinking” process, and the same mechanism is used during training and inference.

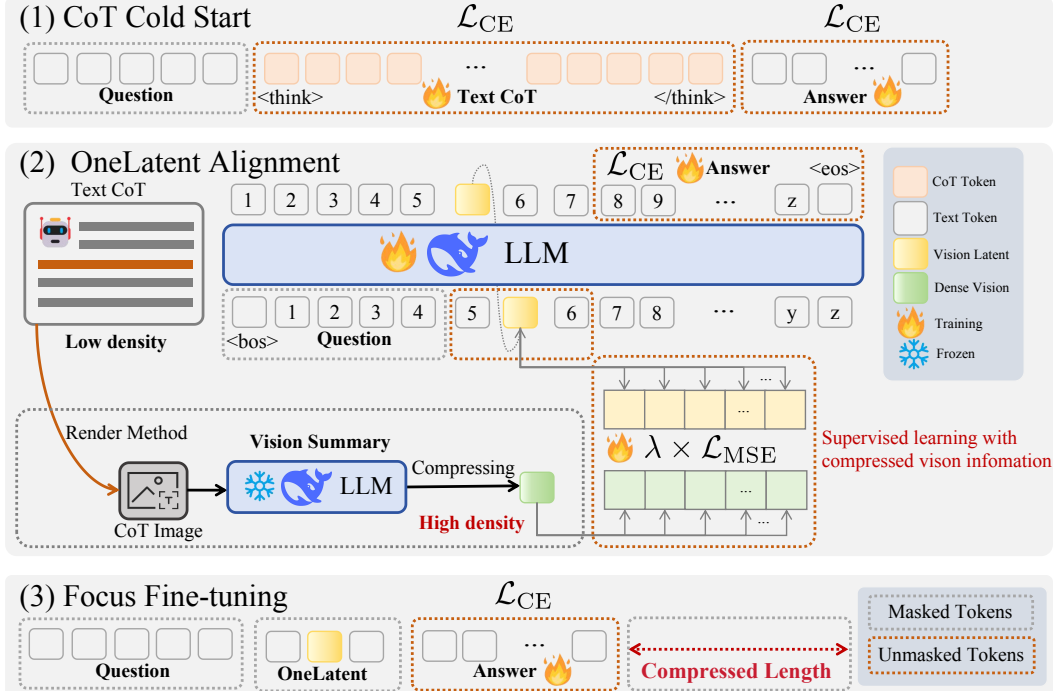


Figure 2: Three-stage training pipeline of OneLatent. Stage 1 trains explicit CoT generation with cross-entropy. Stage 2 replaces CoT with one latent token and adds MSE alignment to pre-extracted visual hidden-state targets. Stage 3 keeps the one-latent interface and trains answer generation without alignment loss. The figure shows the supervision shift from explicit textual CoT to latent alignment and then to answer-only decoding.

### 3.3 Data Preparation and CoT Rendering

Our rendering pipeline follows the `onelatent_gsm8k` implementation. Each CoT trace is rendered into a fixed square canvas ( $W=H=1024$  for standard GSM8K-Aug,  $W=H=512$  for tiny runs), with padding  $p$  and a mono-spaced font (DejaVu/Liberation/FreeMono fallback). We approximate the maximum characters per line by

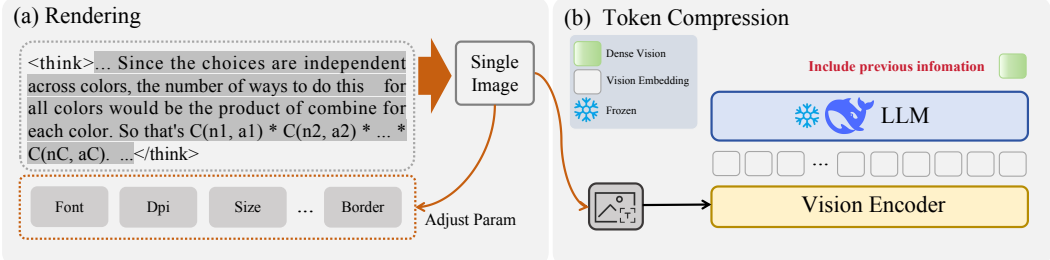
$$m(f) = \left\lfloor \frac{W - 2p}{f/2} \right\rfloor, \quad (3)$$

wrap the text into  $L = \lceil |s|/m(f) \rceil$  lines, and render in black on white. To guarantee that the entire CoT fits inside the fixed canvas, we perform a bounded search over font sizes  $f \in [f_{\min}, f_{\max}]$  and select the largest size that satisfies the height constraint

$$L \cdot (f + g) + 2p \leq H, \quad (4)$$

where  $g$  is a line-gap factor (we use  $g=f/4$ ). This ‘‘fit-to-canvas’’ search is lightweight and deterministic. The result is a single image that preserves the left-to-right reading order while ensuring no truncation.

Figure 3 illustrates the complete data preparation pipeline. The process begins with the original dataset containing questions, explicit CoT reasoning, and answers. We first render each CoT text into a fixed-size image using our deterministic layout algorithm, which automatically adjusts font size to ensure the entire reasoning trace fits within the canvas while maintaining readability. These rendered images are then processed through the DeepSeek-OCR vision-encoder, which consists of frozen SAM-ViT-B and CLIP-L encoders. The visual features are concatenated, projected to the LLM hidden dimension, and forwarded through all LLM layers. We extract the final hidden state at the last position as the target supervision vector  $v \in \mathbb{R}^d$ , which is stored as a target hidden state for use during Stage 2 training. This offline preparation ensures that training requires only text input while maintaining a visual anchor for latent alignment.




---

**Algorithm 1** Deterministic CoT Rendering with OCR-Based Quality Check

---

```

1: Input: CoT string  $s$ , canvas size  $(W, H)$ , padding  $p$ , font range  $[f_{\min}, f_{\max}]$ , DPI range, quality
   threshold  $\tau$ 
2: Initialize:  $\text{DPI} \leftarrow \text{DPI}_{\text{default}}$ ,  $p \leftarrow p_{\text{default}}$ 
3: repeat
4:   for  $f$  from  $f_{\max}$  down to  $f_{\min}$  do
5:      $m \leftarrow \lfloor (W - 2p)/(f/2) \rfloor$ 
6:     wrap  $s$  into  $L$  lines using width  $m$ 
7:     Wrap uses greedy whitespace breaks; overlong tokens fall back to character-level splitting.
8:      $h \leftarrow L \cdot (f + g) + 2p$ 
9:     if  $h \leq H$  then
10:      render image  $I$  with font size  $f$ ,  $\text{DPI}$ , padding  $p$ 
11:      break
12:    end if
13:  end for
14:   $Q \leftarrow \text{DeepSeek-OCR}(I)$  {Compute OCR quality score}
15:  if  $Q < \tau$  then
16:    Adjust  $\text{DPI}$  or padding  $p$  {Increase clarity}
17:  end if
18: until  $Q \geq \tau$  or max iterations reached
19: save image  $I$  (white background, black text)
20: return  $I$ 

```

---

**Quality verification via DeepSeek-OCR.** To ensure rendered images are clear and readable, we employ DeepSeek-OCR [Wei et al., 2025a] as an automatic quality checker. For each rendered image, we use the vision-encoder to verify whether the text is legible. If the OCR confidence score falls below a threshold or text recognition accuracy is poor, we automatically adjust rendering parameters including dots per inch(DPI) and border padding. This iterative refinement process continues until the rendered image achieves satisfactory clarity, ensuring that the visual targets extracted from these images provide stable supervision signals for latent alignment.

**Rendering algorithm.** Algorithm 1 summarizes the procedure used in our preprocessing procedure. We first normalize the CoT string by collapsing whitespace, converting LaTeX-like tokens (e.g., `\times`, `\leq`) into Unicode, and stripping markup that is not part of the reasoning trace. We then select a mono-spaced font (with deterministic fallback order) and compute a conservative characters-per-line budget to preserve left-to-right reading order. A descending search over font sizes ensures the full trace fits in the fixed canvas; if no size satisfies the height constraint, we fall back to the minimum font size and clip only trailing whitespace. This deterministic rendering pipeline makes the image targets reproducible across machines and allows caching during large-scale preprocessing.

### 3.4 Hidden-State Targets via DeepSeek-OCR Encoder

We encode rendered CoT images with the DeepSeek-OCR vision-encoder stack [Wei et al., 2025a]. Each image is padded to the target size, passed through the frozen vision-encoder (SAM-ViT-B and CLIP-L) [Kirillov et al., 2023, Radford et al., 2021], concatenated, and projected to the LLM hidden dimension. We then concatenate a BOS embedding with the visual embeddings and forward through the LLM layers; the final hidden state at the last visual position is used as the target latent vector  $v \in \mathbb{R}^d$ :

$$v = \text{LM}([\text{BOS}; \text{Vision}(I)])_{-1}. \quad (5)$$

For the single-latent regime, each example yields one target vector. The target is stored as `.pt` and used only for MSE supervision in Stage 2.

**Text-only training and inference.** During training and inference, the model never consumes images directly. Instead, precomputed hidden-state targets derived from rendered CoT images are loaded from disk and used only for MSE supervision in Stage 2. This keeps the runtime interface purely textual while retaining a visual anchor during training.

**Patch alignment and OCR-friendly layout.** We favor mono-spaced fonts and fixed margins to keep glyph spacing predictable across samples. This allows the vision-encoder to see stable, left-to-right visual patterns that resemble OCR inputs. Since the downstream supervision target is extracted after the LLM layers, minor pixel-level variations are smoothed by the encoder and projector, but large layout shifts can destabilize training. Empirically, fixed-size canvases with deterministic wrapping produce the most stable alignment loss.

### 3.5 Three-Stage Training Strategy

We train with a three-stage progressive strategy that gradually transforms explicit CoT reasoning into compressed latent representations while ensuring answer quality. Stages 1 and 3 follow standard supervised fine-tuning (SFT) on text sequences (next-token prediction), while Stage 2 augments SFT with an additional latent-alignment loss.

**Stage 1 (CoT Cold Start).** Input sequence:

$$x^{(0)} = [q, <|\text{begin-latent}|>, <|\text{end-latent}|>, r, a],$$

where  $r$  is the explicit CoT text. This is an SFT stage: we optimize NTP on CoT + answer tokens and do not use MSE.

**Stage 2 (OneLatent Alignment).** Input sequence:

$$x^{(1)} = [q, <|\text{begin-latent}|>, <|\text{latent}|>, <|\text{end-latent}|>, a].$$

We optimize NTP on answer tokens and add MSE between the  $<|\text{begin-latent}|>$ hidden state and target  $v$  (SFT + alignment).

**Stage 3 (Focus Fine-tuning).** Input sequence:

$$x^{(2)} = [q, <|\text{begin-latent}|>, <|\text{latent}|>, <|\text{end-latent}|>, a].$$

We drop MSE and continue SFT on answer tokens to consolidate decoding quality.

We optimize next-token prediction (NTP) on the answer tokens and (optionally) CoT tokens:

$$\mathcal{L}_{\text{NTP}} = - \sum_{t \in \mathcal{A}} \log p_{\theta}(x_t | x_{<t}), \quad (6)$$

where  $\mathcal{A}$  denotes supervised token positions (CoT+answer in Stage 1; answer-only in Stages 2 and 3). For latent alignment we use:

$$\mathcal{L}_{\text{MSE}} = \|h_{\text{bot}} - v\|_2^2, \quad (7)$$

which compares the hidden state at the `<|begin-latent|>` position to the pre-extracted target. The total loss is:

$$\mathcal{L} = \begin{cases} \mathcal{L}_{\text{NTP}}, & \text{Stage 1} \\ \mathcal{L}_{\text{NTP}} + \lambda \mathcal{L}_{\text{MSE}}, & \text{Stage 2} \\ \mathcal{L}_{\text{NTP}}, & \text{Stage 3} \end{cases} \quad (8)$$

with  $\lambda = 1$  in our default configuration.

For  $N = 1$ , the MSE aligns the hidden state at the `<|begin-latent|>` position with  $v$  and the latent token is filled with this hidden state during forward pass.

### 3.6 Inference

At inference, we construct the same latent segment and generate only the answer. The latent token is filled by the previous hidden state, and decoding proceeds autoregressively from `<|end-latent|>`.

**Fixed latent length design.** We keep a fixed latent length ( $N = 1$ ) to maintain a deterministic interface and a one-to-one correspondence between each rendered CoT image and its target hidden state. Dynamic latent length would require a separate length predictor and would decouple the latent supervision target from the latent slot being trained, complicating alignment and degrading training stability. Fixed length also guarantees consistent compute and simplifies batching.

**Complexity and efficiency.** Let  $T$  be the answer length and  $N$  the latent length. Autoregressive decoding cost is  $O(T+N)$ , while explicit CoT incurs  $O(T+R)$  with  $R \gg N$ . This is the primary source of inference speedups. Training costs include rendering and visual encoding, but those are offline and do not affect runtime inference.

## 4 Experiments

### 4.1 Experimental Setup

#### 4.1.1 Datasets

We separate training sources from evaluation benchmarks. For training, we use GSM8K-Aug-NL [Deng et al., 2023], an augmented GSM8K [Cobbe et al., 2021] corpus with approximately 385k training samples (used for supervision and latent-target preparation, not as a standalone row in Table 1). For evaluation, we report two settings: (1) five standard reasoning benchmarks (GSM8K, GSM8K-Hard, SVAMP, ProntoQA, ProsQA) in Table 1; and (2) two enhanced long-chain benchmarks (ProntoQA Enhanced, ProsQA Enhanced) in Table 2.

#### 4.1.2 Enhanced Dataset Generation

For enhanced-set evaluation, we use ProntoQA Enhanced (290 test samples, logical reasoning) and ProsQA Enhanced (500 test samples, procedural reasoning). Both contain explicit CoT traces that are rendered into images for visual latent supervision.

**ProntoQA/ProsQA enhanced.** We generate enhanced variants by expanding CoT steps using large language models and validating them through LLM-as-Judge verification to ensure both correctness and sufficient reasoning depth. Algorithm 2 describes the expansion and validation procedure.

Our preprocessing procedure converts LaTeX-like tokens to Unicode and renders each expanded CoT into  $1024 \times 1024$  PNG images. Hidden-state targets are then extracted by processing these images through the vision-encoder to produce a single  $[1, 1280]$  target vector per sample.

**GSM8K-Aug for training.** We do not create a separate “GSM8K-Aug Enhanced” evaluation table in this paper. GSM8K-Aug-NL is used as a training source (and in-stage ablations), while the enhanced evaluation in Table 2 focuses on ProntoQA/ProsQA where reasoning chains are longer and structurally constrained.

---

**Algorithm 2** LLM-Based CoT Expansion with Judge Validation

---

```
1: Input: Original CoT text  $C_0$ , target length  $L_{\text{target}}$ , max iterations  $K$ 
2: Output: Validated expanded CoT  $C^*$ 
3:  $C \leftarrow C_0$ 
4: for  $k = 1$  to  $K$  do
5:   if  $|C| \geq L_{\text{target}}$  then
6:     break
7:   end if
8:    $C' \leftarrow \text{LLM}_{\text{expand}}(C)$  {Prompt LLM to add intermediate steps}
9:   valid  $\leftarrow \text{LLM}_{\text{judge}}(C', \text{original\_answer})$  {Verify correctness}
10:  if valid then
11:     $C \leftarrow C'$ 
12:  else
13:    continue {Reject invalid expansion, retry}
14:  end if
15: end for
16:  $C^* \leftarrow C$ 
17: return  $C^*$ 
```

---

**Rendering configuration.** We use  $1024 \times 1024$  PNG images with white background, black text, and mono-spaced font (Courier New). The font size is automatically adjusted via the fit-to-canvas search in Algorithm 1 to ensure CoT text fits within the image boundaries. Border padding is set to 20 pixels, and DPI is fixed at 100 for consistent rendering across all datasets.

#### 4.1.3 Training Details

We use the DeepSeek-OCR LLM as the base model. Training defaults follow the training configuration: 15 epochs per stage, batch size 1 per GPU, and learning rate  $2 \times 10^{-5}$  with AdamW. Special tokens  $\langle|\text{begin-latent}|>$ ,  $\langle|\text{latent}|>$ ,  $\langle|\text{end-latent}|>$  are added to the tokenizer, and their embeddings are initialized to the mean embedding. Hidden-state targets are loaded from precomputed .pt files. We train with 8 GPUs using distributed data parallelism and evaluate on held-out validation samples after each epoch.

#### 4.1.4 Evaluation Protocol

We report exact-match accuracy after normalization (e.g., GSM8K uses the standard “###” answer extraction; ProntoQA/ProQA compare the normalized final sentence). Our evaluation procedure reports accuracy in percent; for ProntoQA/ProQA we convert fractional accuracy to percent. We also report average input/output token counts from the evaluation logs. We introduce a new metric, **Output Token Contribution (OTC)**, defined as

$$\text{OTC} = \frac{\text{Acc}}{\text{AvgOut}}, \quad (9)$$

where Acc is accuracy in percent and AvgOut is the average generated output tokens. Higher OTC indicates better accuracy per generated token.

## 4.2 Results

### 4.2.1 Main Results

Table 1 compares OneLatent against four baselines (No CoT, iCoT, CoT, COCONUT) across five reasoning benchmarks. Three trends are clear. (1) **Efficiency under constrained decoding:** OneLatent reduces average output length from 74.62 tokens (CoT) to 6.78 tokens with one latent token, while maintaining high OTC (7.77 average). (2) **Competitive long-chain performance:** OneLatent reaches 99.80% on ProntoQA and 97.80% on ProQA with OTC 10.06 and 11.10, respectively. (3) **Trade-off profile vs iCoT reference logs:** iCoT remains competitive on selected efficiency points, but trails on math-heavy sets (GSM8K-H: 4.30%, SVAMP: 22.50%) and has lower average accuracy (41.4%) than OneLatent (52.7%). Overall, OneLatent provides a stronger accuracy-efficiency balance with a fixed single-latent interface.

Table 1: Method comparison across five reasoning datasets. Metrics: Acc = Accuracy (%), #O = Average output tokens (including latent), #L = Number of latent tokens, OTC = Output Token Contribution (Acc/#O, higher is better). Results shown as mean $\pm$ std.

	GSM8K		GSM8K-H		SVAMP		ProntoQA		ProsQA		AVG	
	Acc #O	OTC #L	Acc #O	OTC #L	Acc #O	OTC #L	Acc #O	OTC #L	Acc #O	OTC #L	Acc #O	OTC #L
No CoT	5.76 $\pm$ .18 2.00 $\pm$ .00	2.88 $\pm$ .09 —	1.36 $\pm$ .09 4.63 $\pm$ .00	0.29 $\pm$ .02 —	5.00 $\pm$ .16 4.04 $\pm$ .00	1.24 $\pm$ .04 —	91.0 $\pm$ .32 9.47 $\pm$ .00	9.61 $\pm$ .03 —	60.4 $\pm$ .28 8.55 $\pm$ .00	7.06 $\pm$ .03 —	32.7 $\pm$ .21 5.74 $\pm$ .00	5.70 $\pm$ .04 —
iCoT	7.81 $\pm$ .74 2.00 $\pm$ .04	3.91 $\pm$ .38 —	4.30 $\pm$ .56 4.59 $\pm$ .06	0.94 $\pm$ .12 —	22.50 $\pm$ .132 7.06 $\pm$ .08	3.19 $\pm$ .19 —	84.8 $\pm$ .161 9.81 $\pm$ .14	8.64 $\pm$ .20 —	87.4 $\pm$ .148 6.82 $\pm$ .12	12.8 $\pm$ .31 —	41.4 $\pm$ .54 6.06 $\pm$ .04	6.84 $\pm$ .10 —
CoT	40.5 $\pm$ .35 31.0 $\pm$ .26	1.31 $\pm$ .02 —	11.3 $\pm$ .23 100 $\pm$ .12	0.11 $\pm$ .00 —	52.0 $\pm$ .38 88.0 $\pm$ .94	0.59 $\pm$ .01 —	94.5 $\pm$ .29 121 $\pm$ .18	0.78 $\pm$ .01 —	76.2 $\pm$ .31 33.3 $\pm$ .42	2.29 $\pm$ .03 —	54.9 $\pm$ .31 74.6 $\pm$ .92	0.74 $\pm$ .01 —
COCONUT	28.5 $\pm$ .29 10.8 $\pm$ .18	2.64 $\pm$ .05 6	6.90 $\pm$ .19 10.9 $\pm$ .21	0.63 $\pm$ .02 6	40.0 $\pm$ .34 11.0 $\pm$ .19	3.64 $\pm$ .07 6	94.4 $\pm$ .28 16.8 $\pm$ .34	5.63 $\pm$ .12 6	89.2 $\pm$ .33 13.5 $\pm$ .28	6.60 $\pm$ .14 6	51.8 $\pm$ .29 12.6 $\pm$ .24	4.11 $\pm$ .08 6
OneLatent	24.8 $\pm$ .24 5.09 $\pm$ .08	4.87 $\pm$ .09 1	4.58 $\pm$ .15 5.10 $\pm$ .09	0.90 $\pm$ .03 1	36.5 $\pm$ .32 5.00 $\pm$ .07	7.30 $\pm$ .12 1	99.8 $\pm$ .08 9.92 $\pm$ .16	10.1 $\pm$ .16 1	97.8 $\pm$ .12 8.81 $\pm$ .14	11.1 $\pm$ .18 1	52.7 $\pm$ .18 6.78 $\pm$ .11	7.77 $\pm$ .13 1

**iCoT-specific comparison.** Compared with iCoT, OneLatent improves accuracy on all five reported datasets: +16.99 (GSM8K), +0.28 (GSM8K-H), +14.00 (SVAMP), +15.00 (ProntoQA), and +10.40 (ProsQA) percentage points. iCoT is strongest in ultra-short decoding regimes (e.g., 2.00 output tokens on GSM8K and 6.82 on ProsQA), which explains its high OTC on ProsQA. However, this aggressive compression is less stable on arithmetic-heavy benchmarks, where OneLatent achieves substantially higher accuracy while retaining strong OTC. This pattern is consistent with our MDL intuition: compact descriptions help only when they remain task-sufficient.

Table 2: OneLatent compression results on enhanced datasets. Metrics: #OA = Original Accuracy (%), CoT baseline), #NA = New Accuracy (%), OneLatent), #CO = CoT Output Tokens, #NO = New Output Tokens (OneLatent), #CR = Compression Ratio (#CO/#NO). Results shown as mean $\pm$ std.

Dataset	#OA (%)	#NA (%)	#CO	#NO	#CR
ProntoQA Enhanced	99.80 $\pm$ .08	99.90 $\pm$ .06	784.50 $\pm$ 5.2	8.98 $\pm$ .18	87.4 $\times$
ProsQA Enhanced	97.80 $\pm$ .12	98.10 $\pm$ .10	804.84 $\pm$ 6.8	9.98 $\pm$ .21	80.6 $\times$

Table 2 shows OneLatent performance on the two enhanced evaluation datasets (ProntoQA Enhanced and ProsQA Enhanced). OneLatent maintains strong accuracy while keeping outputs short, indicating effective latent compression of reasoning.

**Cross-dataset trends.** Across the five standard benchmarks in Table 1, OneLatent is strongest on long-chain logical tasks (ProntoQA/ProsQA) and shows larger trade-offs on arithmetic-heavy tasks (especially GSM8K-Hard and SVAMP). Table 2 further shows large compression ratios on enhanced logical sets (87.4 $\times$  on ProntoQA Enhanced and 80.6 $\times$  on ProsQA Enhanced).

**Interpreting OTC.** OTC surfaces regimes where accuracy is achieved with minimal decoding. For example, ProntoQA shows high OTC despite short outputs, indicating that latent compression concentrates reasoning in hidden states rather than in emitted tokens. From an MDL perspective, OTC is a practical proxy for “correctness per emitted description length” at inference time, complementing absolute accuracy when evaluating compressed reasoning interfaces.

**Enhanced-set comparison.** On the two enhanced evaluation sets, OneLatent retains high accuracy with short outputs, indicating that single-latent compression remains effective when reasoning traces are long.

#### 4.2.2 Ablation

Table 3 shows the three-stage training progression on GSM8K, ProntoQA, and ProsQA. Stage 1 (CoT Cold Start) establishes baseline reasoning with explicit CoT generation, achieving 19.63% on GSM8K,

48.28% on ProntoQA, and 49.00% on ProsQA, but with high output lengths (24.26, 120.73, and 33.28 tokens respectively) and low OTC scores (0.81, 0.40, and 1.47). Stage 2 (OneLatent Alignment) introduces single-token latent supervision, dramatically improving efficiency: OTC increases by 4.8 $\times$  on GSM8K (0.81  $\rightarrow$  3.87), 23.5 $\times$  on ProntoQA (0.40  $\rightarrow$  9.39), and 6.9 $\times$  on ProsQA (1.47  $\rightarrow$  10.18), while reducing output length by 78.3%, 91.8%, and 73.5% respectively. Stage 3 (Focus Fine-tuning) further improves accuracy without latent supervision: GSM8K reaches 24.79% (+4.40 from Stage 2), ProntoQA reaches 99.80% (+6.60), and ProsQA reaches 97.80% (+8.00), achieving the final OTC scores of 4.87, 10.06, and 11.10. The progressive training demonstrates that (1) latent alignment is critical for compressing reasoning into a single token, and (2) answer-focused fine-tuning consolidates the latent representation while improving task accuracy.

Table 3: Ablation study: three-stage training progression. Metrics: Acc = Accuracy (%), Avg Out = Average output tokens, Latents = Number of latent tokens, OTC = Output Token Contribution (Acc/Avg Out). Results shown as mean $\pm$ std. Stage 1 = CoT Cold Start, Stage 2 = OneLatent Alignment, Stage 3 = Focus Fine-tuning (final).

Dataset	Stage	Acc (%)	Avg Out	Latents	OTC
GSM8K	Stage 1 (CoT)	19.63 $\pm$ .22	24.26 $\pm$ .38	0	0.81 $\pm$ .02
	Stage 2 (Alignment)	20.39 $\pm$ .23	5.26 $\pm$ .11	1	3.87 $\pm$ .09
	Stage 3 (Final)	<b>24.79</b> $\pm$ .24	<b>5.09</b> $\pm$ .08	1	<b>4.87</b> $\pm$ .09
ProntoQA	Stage 1 (CoT)	48.28 $\pm$ .36	120.73 $\pm$ 1.8	0	0.40 $\pm$ .01
	Stage 2 (Alignment)	93.20 $\pm$ .18	9.92 $\pm$ .16	1	9.39 $\pm$ .16
	Stage 3 (Final)	<b>99.80</b> $\pm$ .08	<b>9.92</b> $\pm$ .16	1	<b>10.06</b> $\pm$ .18
ProsQA	Stage 1 (CoT)	49.00 $\pm$ .37	33.28 $\pm$ .42	0	1.47 $\pm$ .03
	Stage 2 (Alignment)	89.80 $\pm$ .26	8.82 $\pm$ .15	1	10.18 $\pm$ .19
	Stage 3 (Final)	<b>97.80</b> $\pm$ .12	<b>8.81</b> $\pm$ .14	1	<b>11.10</b> $\pm$ .20

### 4.3 Discussion

**Token efficiency.** On the enhanced logical sets, OneLatent achieves large compression ratios (87.4 $\times$  on ProntoQA Enhanced and 80.6 $\times$  on ProsQA Enhanced). On the five standard benchmarks, it maintains short outputs with a fixed single latent token, reducing key-value cache growth from long textual CoT traces and improving throughput in batch inference.

**Accuracy trade-offs.** Logical reasoning tasks benefit more from latent alignment than arithmetic-heavy tasks. This pattern is consistent in both the main comparison and the staged ablations.

**Inference efficiency.** Because decoding cost scales linearly with generated tokens, reductions in output length translate directly into latency and memory savings. The latent token itself incurs a constant overhead ( $N=1$ ) and does not grow with reasoning length. With fixed latent length, the KV cache grows primarily with answer tokens rather than reasoning tokens, making OneLatent particularly attractive for long-context deployments where explicit CoT would otherwise dominate memory usage.

**Limitations.** OneLatent relies on accurate rendered CoT supervision. Errors in the CoT or rendering pipeline can propagate into the latent representation. The method also depends on a specific DeepSeek-OCR vision-encoder and a fixed rendering resolution; generalizing to other domains may require re-tuning. Finally, latent reasoning reduces transparency: while it improves efficiency, it complicates debugging and interpretability, which remain open challenges.

## 5 Conclusion

This paper studies reasoning compression through an MDL motivation: when different explanations yield the same answer, shorter sufficient descriptions should generalize better under constrained decoding. We operationalize this idea with OneLatent, which compresses explicit CoT into a single latent token supervised by DeepSeek-OCR-derived hidden states.

The empirical results are consistent with this intuition. OneLatent achieves  $11\times$  average output compression, reaches a peak compression ratio of  $87.4\times$ , and improves OTC by  $6.8\times$  over textual CoT with only a 2.21% average accuracy drop across five benchmarks. On long-chain logical reasoning, it achieves strong accuracy with one latent token. Error shifts are concentrated in arithmetic-heavy settings, suggesting that compression primarily removes redundant verbalization rather than uniformly degrading reasoning performance.

Together, these findings indicate that compression is not only an efficiency tool, but also a useful inductive constraint for stable reasoning under limited output budgets. OTC is a practical MDL-motivated efficiency proxy for this regime. This paper reports ongoing work, and these results should be viewed as an intermediate step.

## References

Jiale Cheng, Yusen Liu, Xinyu Zhang, Yulin Fei, Wenyi Hong, Ruiliang Lyu, Weihan Wang, Zhe Su, Xiaotao Gu, Xiao Liu, Yushi Bai, Jie Tang, Hongning Wang, and Minlie Huang. Glyph: Scaling context windows via visual-text compression, 2025. URL <https://arxiv.org/abs/2510.17800>.

Karl Cobbe, Vineet Kosaraju, Mohammad Bavarian, Mark Chen, Heewoo Jun, Lukasz Kaiser, Matthias Plappert, Jerry Tworek, Jacob Hilton, Reiichiro Nakano, et al. Training verifiers to solve math word problems. *arXiv preprint arXiv:2110.14168*, 2021.

Yuntian Deng, Kiran Prasad, Roland Fernandez, Paul Smolensky, Vishrav Chaudhary, and Stuart Shieber. Implicit chain of thought reasoning via knowledge distillation. *arXiv preprint arXiv:2311.01460*, 2023.

Yuntian Deng, Yejin Choi, and Stuart Shieber. From explicit cot to implicit cot: Learning to internalize cot step by step. *arXiv preprint arXiv:2405.14838*, 2024.

Sachin Goyal, Ziwei Ji, Ankit Singh Rawat, Aditya Krishna Menon, Sanjiv Kumar, and Vaishnavh Nagarajan. Think before you speak: Training language models with pause tokens. *arXiv preprint arXiv:2310.02226*, 2023.

Peter Grünwald and Teemu Roos. Minimum description length revisited. *International Journal of Mathematics for Industry*, 11(01), December 2019. ISSN 2661-3344. doi: 10.1142/s2661335219300018. URL <http://dx.doi.org/10.1142/S2661335219300018>.

Shibo Hao, Yi Gu, Haodi Ma, Joshua Jiahua Hong, Zhen Wang, Daisy Zhe Wang, and Zhiting Hu. Reasoning with language model is planning with world model. *arXiv preprint arXiv:2305.14992*, 2023.

Shibo Hao, Yi Gu, Haotian Luo, Tianyang Liu, Xiyan Shao, Xinyuan Wang, Shuhua Xie, Haodi Ma, Adithya Samavedhi, Qiyue Gao, et al. Llm reasoners: New evaluation, library, and analysis of step-by-step reasoning with large language models. *arXiv preprint arXiv:2404.05221*, 2024.

Shibo Hao, Sainbayar Sukhbaatar, DiJia Su, Xian Li, Zhiting Hu, Jason Weston, and Yuandong Tian. Training large language models to reason in a continuous latent space, 2025. URL <https://arxiv.org/abs/2412.06769>.

Tushar Khot, Harsh Trivedi, Matthew Finlayson, Yao Fu, Kyle Richardson, Peter Clark, and Ashish Sabharwal. Decomposed prompting: A modular approach for solving complex tasks. *arXiv preprint arXiv:2210.02406*, 2022.

Alexander Kirillov, Eric Mintun, Nikhila Ravi, Hanzi Mao, Chloe Rolland, Laura Gustafson, Tete Xiao, Spencer Whitehead, Alexander C. Berg, Wan-Yen Lo, Piotr Dollar, and Ross Girshick. Segment anything, 2023. URL <https://arxiv.org/abs/2304.02643>.

Aman Madaan and Amir Yazdanbakhsh. Text and patterns: For effective chain of thought, it takes two to tango. *arXiv preprint arXiv:2209.07686*, 2022.

Aman Madaan, Niket Tandon, Prakhar Gupta, Skyler Hallinan, Luyu Gao, Sarah Wiegreffe, Uri Alon, Nouha Dziri, Shrimai Prabhumoye, Yiming Yang, et al. Self-refine: Iterative refinement with self-feedback. *Advances in Neural Information Processing Systems*, 36, 2023.

Jacob Pfau, William Merrill, and Samuel R Bowman. Let's think dot by dot: Hidden computation in transformer language models. *arXiv preprint arXiv:2404.15758*, 2024.

Alec Radford, Jong Wook Kim, Chris Hallacy, Aditya Ramesh, Gabriel Goh, Sandhini Agarwal, Girish Sastry, Amanda Askell, Pamela Mishkin, Jack Clark, Gretchen Krueger, and Ilya Sutskever. Learning transferable visual models from natural language supervision, 2021. URL <https://arxiv.org/abs/2103.00020>.

Noah Shinn, Federico Cassano, Ashwin Gopinath, Karthik Narasimhan, and Shunyu Yao. Reflexion: Language agents with verbal reinforcement learning. *Advances in Neural Information Processing Systems*, 36, 2023.

Zayne Sprague, Fangcong Yin, Juan Diego Rodriguez, Dongwei Jiang, Manya Wadhwa, Prasann Singhal, Xinyu Zhao, Xi Ye, Kyle Mahowald, and Greg Durrett. To cot or not to cot? chain-of-thought helps mainly on math and symbolic reasoning. *arXiv preprint arXiv:2409.12183*, 2024.

Miles Turpin, Julian Michael, Ethan Perez, and Samuel Bowman. Language models don't always say what they think: unfaithful explanations in chain-of-thought prompting. *Advances in Neural Information Processing Systems*, 36, 2024.

Karthik Valmeekam, Matthew Marquez, Sarath Sreedharan, and Subbarao Kambhampati. On the planning abilities of large language models-a critical investigation. *Advances in Neural Information Processing Systems*, 36:75993–76005, 2023.

Boshi Wang, Sewon Min, Xiang Deng, Jiaming Shen, You Wu, Luke Zettlemoyer, and Huan Sun. Towards understanding chain-of-thought prompting: An empirical study of what matters. *arXiv preprint arXiv:2212.10001*, 2022a.

Peiyi Wang, Lei Li, Zhihong Shao, Runxin Xu, Damai Dai, Yifei Li, Deli Chen, Yu Wu, and Zhifang Sui. Math-shepherd: Verify and reinforce llms step-by-step without human annotations. In *Proceedings of the 62nd Annual Meeting of the Association for Computational Linguistics (Volume 1: Long Papers)*, pages 9426–9439, 2024.

Xinyi Wang, Lucas Caccia, Oleksiy Ostapenko, Xingdi Yuan, William Yang Wang, and Alessandro Sordoni. Guiding language model reasoning with planning tokens. *arXiv preprint arXiv:2310.05707*, 2023.

Xuezhi Wang, Jason Wei, Dale Schuurmans, Quoc Le, Ed Chi, Sharan Narang, Aakanksha Chowdhery, and Denny Zhou. Self-consistency improves chain of thought reasoning in language models. *arXiv preprint arXiv:2203.11171*, 2022b.

Haoran Wei, Yaofeng Sun, and Yukun Li. Deepseek-ocr: Contexts optical compression, 2025a. URL <https://arxiv.org/abs/2510.18234>.

Jason Wei, Xuezhi Wang, Dale Schuurmans, Maarten Bosma, Fei Xia, Ed Chi, Quoc V Le, Denny Zhou, et al. Chain-of-thought prompting elicits reasoning in large language models. *Advances in neural information processing systems*, 35:24824–24837, 2022.

Xilin Wei, Xiaoran Liu, Yuhang Zang, Xiaotao Dong, Yuhang Cao, Jiaqi Wang, Xipeng Qiu, and Dahua Lin. Sim-cot: Supervised implicit chain-of-thought, 2025b. URL <https://arxiv.org/abs/2509.20317>.

Sean Welleck, Amanda Bertsch, Matthew Finlayson, Hailey Schoelkopf, Alex Xie, Graham Neubig, Ilia Kulikov, and Zaid Harchaoui. From decoding to meta-generation: Inference-time algorithms for large language models. *arXiv preprint arXiv:2406.16838*, 2024.

Yuxi Xie, Kenji Kawaguchi, Yiran Zhao, James Xu Zhao, Min-Yen Kan, Junxian He, and Michael Xie. Self-evaluation guided beam search for reasoning. *Advances in Neural Information Processing Systems*, 36, 2023.

Shunyu Yao, Dian Yu, Jeffrey Zhao, Izhak Shafran, Tom Griffiths, Yuan Cao, and Karthik Narasimhan. Tree of thoughts: Deliberate problem solving with large language models. *Advances in Neural Information Processing Systems*, 36, 2023.

Eric Zelikman, Georges Harik, Yijia Shao, Varuna Jayasiri, Nick Haber, and Noah D Goodman. Quiet-star: Language models can teach themselves to think before speaking. *arXiv preprint arXiv:2403.09629*, 2024.

Denny Zhou, Nathanael Schärli, Le Hou, Jason Wei, Nathan Scales, Xuezhi Wang, Dale Schuurmans, Claire Cui, Olivier Bousquet, Quoc Le, et al. Least-to-most prompting enables complex reasoning in large language models. *arXiv preprint arXiv:2205.10625*, 2022.